Acta Crystallographica Section D
Biological Crystallography
ISSN 0907-4449

Structure determination of porcine haemoglobin

Tian-Huey Lu,[a]* Kaliyamoorthy Panneerselvam,[a] Yen-Chywan Liaw,[b] Pei Kan[c] and Chau-Jen Lee[c]

[a]Department of Physics, National Tsing-Hua University, Hsinchu 30043, Taiwan, [b]Crystallography Laboratory, Institute of Molecular Biology, Academia Sinica, Nankang, Taipei 11529, Taiwan, and [c]Department of Chemical Engineering, National Tsing-Hua University, Hsinchu 30043, Taiwan

Correspondence e-mail: thlu@phys.nthu.edu.tw

Received 18 January 1999
Accepted 5 January 2000

This paper is dedicated to the memory of the late Professor Chau-Jen Lee.

PDB Reference: porcine haemoglobin, 1qpw.

To investigate a potential candidate material for making artificial red blood cells to supplement blood transfusion, the X-ray structure of porcine haemoglobin at 1.8 Å resolution was determined as part of research towards synthesizing human blood. Porcine haemoglobin was crystallized by the vapor-diffusion method, producing crystals of dimensions 0.3–0.5 mm after successive seeding. The crystals belong to the orthorhombic space group $P2_12_12_1$, with unit-cell parameters a = 68.10, b = 72.27, c = 114.85 Å. The initial phase was determined by the molecular-replacement method, using human oxyhaemoglobin as a model. The final R factor was 21.1% for 36 820 reflections after validation of 574 water molecules. The r.m.s. deviations of bond lengths, angles, torsion angles and improper angles from their ideal values are 0.017 Å, 3.0, 20.6 and 1.8°, respectively. The average B factor is 33.63 Å^2 for the haemoglobin molecule and 50.53 Å^2 for the water molecules. The structure could be superimposed on a 2.8 Å resolution structure with an r.m.s. difference of 0.59 Å in main-chain atomic positions and 1.27 Å in side-chain atomic positions. Porcine and human haemoglobins are compared. A tentative model for artificial blood is proposed based on the complementarity relationship of the surface charges between haemoglobin and the surrounding cell membrane.

1. Introduction

Haemoglobin (Hb) based blood substitutes, made of natural oxygen-carrier proteins which are present in red blood cells and are responsible for the transport of oxygen and partly carbon dioxide *in vivo*, fit the demands of human transfusion excellently (Vandegriff & Winslow, 1991). To avoid the transmission of human viruses contaminating outdated blood, animal and recombinant Hbs are increasingly being considered as possible sources. Therefore, Lee *et al.* (1992) have attempted to develop porcine Hb-based blood substitutes, as there is an abundant porcine market in Asia. The results obtained indicated the potential of the novel material for application in medical treatment (Lee *et al.*, 1992; Kan & Lee, 1994; Wang *et al.*, 1996). However, immunological problems of xenogenic infusion and the delicate regulation of oxygen capacity of porcine Hb retarded further clinical applications. Fundamental research regarding the molecular structure and function of porcine Hb is needed in order to work out a safe and effective modification in order to proceed with porcine Hb-based blood substitutes.

The allosteric properties and oxygen-transport characteristics of haemoglobin have attracted considerable study. Many papers have been published on the elucidation of the structure–function relationships of haemoglobins (Bolton &

Perutz, 1970; Frier & Perutz, 1977; Ladner *et al.*, 1977; Braunitzer *et al.*, 1978; Perutz, 1978; Feola *et al.*, 1983; Shaanan, 1983; Fermi *et al.*, 1984, 1992; Ackers & Smith, 1987; Kleinschmidt & Sgouros, 1987; Ippolito *et al.*, 1990; Ryan *et al.*, 1990; Waller & Liddington, 1990; Wireko & Abraham, 1991; Camardella *et al.*, 1992; Coghlan *et al.*, 1992; Kolatkar *et al.*, 1992; Silva *et al.*, 1992; Yamauchi *et al.*, 1992; Perutz *et al.*, 1993; Richard *et al.*, 1993; Braden *et al.*, 1994; Borgstahl *et al.*, 1994*a*,*b*; Condon & Royer, 1994; Moulton *et al.*, 1994; Katz *et al.*, 1994; Osawa *et al.*, 1994; Rizzi *et al.*, 1994; Royer, 1994; Clement *et al.*, 1995; Kavanaugh *et al.*, 1995; Mitchell, Ernst & Hackert, 1995; Mitchell, Ernst, Wu *et al.*, 1995; Pellegrini *et al.*, 1995; Royer *et al.*, 1995; Yang *et al.*, 1995; Pechik *et al.*, 1996; Paoli *et al.*, 1996; Zhang *et al.*, 1996).

We initiated the three-dimensional structure determination of procine haemoglobin (Hsieh *et al.*, 1992) as part of research work on this project. Purified stroma-free haemoglobin extracted from domestic porcine blood is a potential candidate material for making artificial red blood cells to supplement blood transfusion (Lee *et al.*, 1992). Although the structure of aquomet porcine haemoglobin (pHb) has been published (Katz *et al.*, 1994), this was only presented at the resolution of 2.8 Å. Several large uncertainties could not be resolved owing to the inadequate resolution. The X-ray structure determination of domestic pig haemoglobin at 1.8 Å resolution is presented here in order to resolve these structural uncertainties. Many interesting structural differences between pHb and human haemoglobin (hHb) have been discovered.

2. Materials and methods

2.1. Isolation and purification

Fresh porcine whole blood obtained from a slaughterhouse was mixed with 1/10 volume of sodium citrate to avoid blood clotting. Red blood cells, isolated from whole blood by centrifugation (Hitachi centrifuge, Himac CR20B2) at 5000 rev min^{-1} for 15 min, were washed three times with two volumes of 0.9%(*w*/*v*) saline and then haemolyzed by adding three volumes of deionized water. Subsequent centrifugation at 15 000*g* for 60 min yielded Hb solution free of visible cell debris. The solution was mixed with stock solutions of PEG 1500 and K_2HPO_4/NaH_2PO_4 to obtain a solution containing 12.5% PEG, 12.5% phosphate pH 10 with the addition of a small amount of NaOH. After phase separation, the top phase was withdrawn and added to NaH_2PO_4 to a final composition of 12.5% PEG, 12.5% phosphate pH 7. After mixing and phase separation, the bottom phase containing Hb was dialyzed with deionized water to remove surplus phosphate. Porcine Hb powder was obtained by lyophilization and was stored at 253 K.

2.2. Crystallization and data collection

Crystallization of porcine haemoglobin was carried out at room temperature using the vapour-diffusion method (McPherson, 1982) under conditions described previously (Blow, 1958). The purified haemoglobin was dissolved in distilled water and an 80 mg ml^{-1} solution was prepared. 2.8 *M* phosphate solution was used as precipitant (made by mixing K_2HPO_4 and NaH_2PO_4 in the molar ratio 1.35:1.00 at pH 6.8). The crystallization conditions were first investigated by vapour diffusion in hanging drops. After small crystals were grown, the sitting-drop vapour-diffusion method was used. Large drops containing 10 µl of protein and 12 µl of 2.8 *M* phosphate solution were used in the sitting drops, with 10 ml phosphate solution in the reservoir. Small seed crystals were successively transferred between equilibrating protein solutions in spot plates until the crystals grew to dimensions of 0.3–0.5 mm. For X-ray analysis, a suitable crystal was mounted in a thin-walled glass capillary with a small amount of mother liquor to prevent dryness and was sealed with diffusion-pump oil.

Data were collected on an R-AXIS II imaging-plate detector system using Cu $K\alpha$ radiation generated by a Rigaku RU-300 rotating-anode generator operating at a voltage of 50 kV and a current of 80 mA. The crystal-to-detector distance was set to 100 mm. Intensity data were processed using a software package supplied by the Molecular Structure Corporation. A summary of the data-collection statistics is given in Table 1.

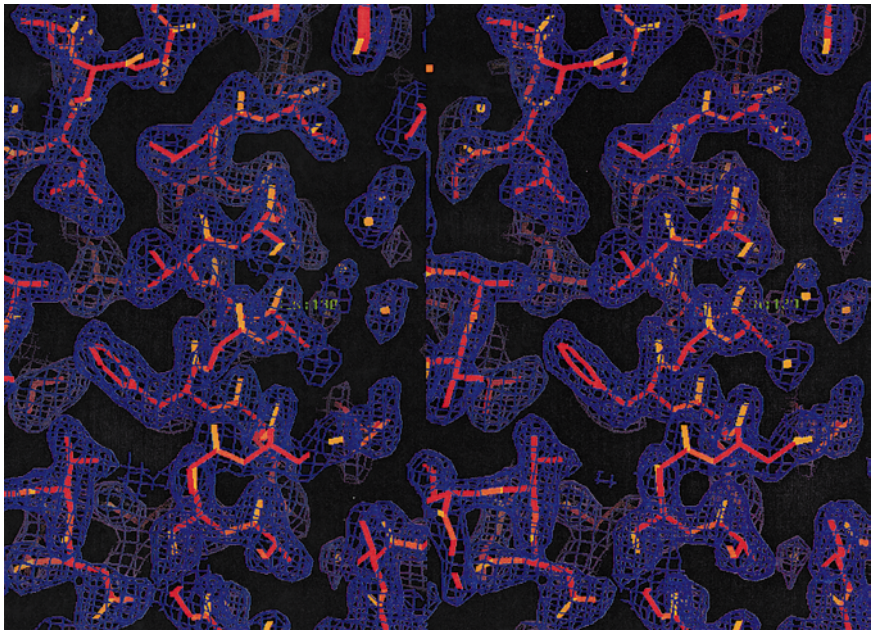

Figure 1
A stereoview of the $2F_o - F_c$ map of the H helix in the α_1 subunit. This shows that the model is of good quality and fits the electron-density map because of the high resolution (1.8 Å).

2.3. Structure solution and refinement

X-PLOR (Brünger, 1992) was used for the structure determination of pHb. In the investigation of the spacial orientation relationship between the $\alpha_1\beta_1$ dimer and the $\alpha_2\beta_2$ dimer of the pHb tetramer, the

Table 1
Statistics for pHb.

(*a*) Data collection.

Space group	$P2_12_12_1$
Unit-cell parameters (Å)	a = 68.10 (1), b = 72.27 (1), c = 114.85 (2)
Resolution range (Å)	8.0–1.8 (1.88–1.8)†
No. of unique reflections	37481 (1068)†
R_{merge}‡ (%)	5.8

(*b*) Intensity statistics.

Resolution range (Å)	Observed reflections	Theoretical reflections	Completeness (%)
8.00–3.60	6668	6976	95.6
3.60–2.55	11495	12229	94.0
2.55–2.08	13025	15522	83.9
2.08–1.80	6277	18346	34.2

† Figures given in parentheses are values for the last resolution shell. ‡ $R_{merge} = \sum|I - \langle I\rangle| / \sum|\langle I\rangle|$, where $\langle I\rangle$ is the mean intensity of a set of equivalent reflections and the summation is over the reflections with $I/\sigma(I) > 1.0$.

Table 2
Refinement parameters of the final model.

Resolution range (Å)	8.0–1.8
σ cutoff applied	$2\sigma(F)$
No. of reflections	36820
R factor (all data included) (%)	21.1
R_{work} (90% data) (%)	20.7
R_{free} (%)	25.1
Total No. of non-H atoms	5152
No. of protein atoms	4398
No. of haem atoms	180
No. of water molecules	574
R.m.s. deviations from ideal geometry†	
Bond length (Å)	0.017
Bond angles (°)	3.0
Torsion angles (°)	20.6
Improper angles (°)	1.8
Average B values† (Å^2)	
All atoms	34.8
All protein atoms	32.6
Main-chain atoms	31.4
Side-chain atoms	34.0
Water molecules	50.5

† From the *X-PLOR* program.

self-rotation function (Rossmann & Blow, 1962) was calculated. To obtain the initial phases for the electron-density map, the molecular-replacement method was then applied using human oxyhaemoglobin (hHb; Shaanan, 1983) as the model. The atomic coordinates of the entire tetramer were modified so that all non-identical residues between hHb and pHb were substituted with glycine in the cross-rotation searches. Coordinates files for oxy-hHb were obtained from the Protein Data Bank (Bernstein *et al.*, 1977). The amino-acid identity between hHb and pHb is 84% for the α-subunit and 86% for the β-subunit from a sequence comparison. The top peak from the rotation search was 22σ above the mean, with the next highest peak at 8σ. The rotated dimers were then translated into the unit cell separately, followed by a final translation-search solution for the oriented tetramer, resulting in a conventional crystallographic R factor of 40.2%. Subsequent rigid-body refinement in *X-PLOR*, treating the monomer as an individual rigid body, lowered the R factor to 36.8% for data in the 8.0–3.0 Å resolution range. For this model, simulated-annealing refinement was applied and the R factor fell to 28.5%. The $2F_o - F_c$ and $F_o - F_c$ maps were inspected for further manual intervention using the *QUANTA*97 program (Molecular Simulation Inc., San Diego, USA). After two rounds of major manual intervention, the structure was refined by simulated-annealing refinement using a starting temperature of 3000 K. Each of several rounds of minor manual intervention was followed by positional refinement. The R factor at this stage was 26.2%. Examining the $2F_o - F_c$ electron-density map with peak density >3σ revealed that there was no possibility of finding the phosphate group surrounding this molecule within the distance range 3.5–4.5 Å. Afterwards, provisional positions for water molecules were selected from a $2F_o - F_c$ electron-density map with peak density >3σ; calculated electron densities within 2.6–4.0 Å of the protein were accepted. Subsequent refinement steps with water molecules in these positions, interspersed by examination of the difference maps, validated the positions of 574 water molecules using the cutoff criteria of two hydrogen-bond donors/acceptors within 3.0 Å of the provisional positions and $B < 60$ Å^2. The R factor was reduced to 21.1% for 36 820 reflections with $F > 2\sigma(F)$ in the resolution range 8.0–1.8 Å in the final refinement. Details of the refinement parameters are given in Table 2.

3. Results and discussion

3.1. Quality of the structure

The final model comprises 5152 non-H atoms, representing two $\alpha\beta$ dimer molecules with 574 solvent molecules [treated as O(water) atoms]. Each pHb molecule consists of four polypeptides and four haem groups. The quality of the refinement of pHb has been determined using *PROCHECK* (Laskowski *et al.*, 1993). In the Ramachandran plot, 99.6% residues are in the most favoured and allowed regions, none are in the disallowed regions and only two residues, Asp75 in the α_1 subunit and His77 in the β_1 subunit, are in the generously allowed regions. However, these residues clearly fit the electron-density map well. Other measures of quality applied by *PROCHECK* indicate that the refined parameters, including ω-angles, standard deviations, bad contacts, chirality, hydrogen-bond energies and side-chain torsion angles, are all inside the limits, except for one in a better region derived from well refined structures of comparable resolution. The theoretical estimate of coordinate errors using a Luzzati plot (Luzzati, 1952) is 0.15 Å. The r.m.s. deviations of bond lengths, angles, torsion angles and improper angles from their ideal values are 0.017 Å, 3.0, 20.6 and 1.8°, respectively. The average B factors are 32.63 Å^2 for the pHb molecules and 50.53 Å^2 for the water molecules. A representative electron-density map of the H-helix of the α_1 subunit is shown in Fig. 1. It is clearly obvious that this model fits exactly to the electron-density map owing to the higher resolution (1.8 Å). A comparison of the

structural data between 2.8 Å (Katz *et al.*, 1994) and 1.8 Å resolution is shown in Table 3.

3.2. Secondary structures

The α-subunit of pHb has seven helices (A, B, C, E, F, G and H) and seven non-helical regions, whereas the β-subunit contains eight helical segments (A, B, C, D, E, F, G and H) and seven non-helical regions. This structure has several changes in the helix assignments from those of the 2.8 Å resolution structure; these results are shown in Fig. 2. In general, Pro, Asp, Glu and His residues are not included in the helical region, as the Pro residue is an imino acid and Asp, Glu and His residues carry charges which involve the hydrogen bond to water molecules. However, in the present structure all the above residues are included in the helical region, which also occurs in the structure of ferric soybean leghaemoglobin (Ellis *et al.*, 1997). When this structure was superimposed on the 2.8 Å resolution structure (solved by Katz *et al.*, 1994), the r.m.s. deviation was 0.59 Å for backbone atoms and 1.27 Å for side-chain atoms (Fig. 3). The structures of pHb (1.8 Å) and hHb are quite similar overall; the r.m.s. deviation of all backbone atoms between these two structures is 0.78 Å (Fig. 4), which is similar to the r.m.s. value between the pHb (2.8 Å) and hHb structures. This r.m.s. value is slightly higher than the theoretical value of 0.5 Å calculated from the sequence–structure relationship for homologous proteins (Chothia & Lesk, 1986).

The plots of the least-squares superpositions of the α_1 subunit on the α_2 subunit and the β_1 subunit on the β_2 subunit reveal that the conformations of the α_1 and α_2 subunits and the β_1 and β_2 subunits are similar, except some terminal residues and few intermediate residues. In porcine haemoglobin, the α subunit superimposes upon its sister subunit with r.m.s. deviations of 2.03 Å for side-chain atoms and 0.83 Å for backbone atoms. There are six regions which have major structural differences in the α subunit: two residues in the amino terminal, two residues in the A helix (Val15 and Gly16), two residues in the CE loop (His50 and Gly51), two residues in the EF loop (Asp74 and Asp75), three residues (Asp115, Asp116 and Phe117) in the GH loop and three residues at the C-terminal; there is one minor difference at the end of the

1				5					10	A				15					20
Val	Leu	Ser	Ala	Ala	Asp	Lys	Ala	Asn	Val	Lys	Ala	Ala	Trp	Gly	Lys	Val	Gly	Gly	Gln
NA1	NA2	A1				A5					A10					A15	A16	AB1	B1
				25			B		30					35					40
Ala	Gly	Ala	His	Gly	Ala	Glu	Ala	Leu	Glu	Arg	Met	Phe	Leu	Gly	Phe	Pro	Thr	Thr	Lys
			B5					B10					B15		B17	C1			
C				45					50					55					60
Thr	Tyr	Phe	Pro	His	Phe	Asn	Leu	Ser	His	Gly	Ser	Asp	Gln	Val	Lys	Ala	His	Gly	Gln
C5		C7	CE1				CE5			CE8	E1				E5		distal		
	E			65					70					75					80
Lys	Val	Ala	Asp	Ala	Leu	Thr	Lys	Ala	Val	Gly	His	Leu	Asp	Asp	Leu	Pro	Gly	Aal	Leu
E10					E15					E20	E21	EF1	EF2	F1				F5	
	F			85					90					95					100
Ser	Ala	Leu	Ser	Asp	Leu	His	Ala	His	Lys	Leu	Arg	Val	Asp	Pro	Val	Asn	Phe	Lys	Leu
			F10			proximal		F15	FG1			FG4	G1				G5		
			G	105					110					115					120
Leu	Ser	His	Cys	Leu	Leu	Val	Thr	Leu	Ala	Ala	His	His	Pro	Asp	Asp	Phe	Asn	Pro	Ser
		G10					G15					G20	GH1			GH4	H1		
				125			H		130					135					140
Val	His	Ala	Ser	Leu	Asp	Lys	Phe	Leu	Ala	Asn	Val	Ser	Thr	Val	Leu	Thr	Ser	Lys	Tyr
	H5					H10					H15					H20	H21	HC1	
Arg																			
HC3																			

(*a*)

1				5					1υ	A				15					20
Val	His	Leu	Ser	Ala	Glu	Glu	Lys	Glu	Ala	Val	Leu	Gly	Leu	Trp	Gly	Lys	Val	Asn	Val
NA1		NA3	A1			A5						A10			A14	AB1	AB2	B1	
				25		B			30					35					40
Asp	Glu	Val	Gly	Gly	Glu	Ala	Leu	Gly	Arg	Leu	Leu	Val	Val	Tyr	Pro	Trp	Thr	Gln	Arg
		B5					B10					B15		B17	C1				C5
C				45					50			D		55					60
Phe	Phe	Glu	Ser	Phe	Gly	Asp	Leu	Ser	Asn	Ala	Asp	Ala	Val	Met	Gly	Asn	Pro	Lys	Val
				C10	C11	CD1		CD3	D1				D5		D7	E1			
				65	E				70					75					80
Lys	Ala	His	Gly	Lys	Lys	Val	Leu	Gln	Ser	Phe	Ser	Asp	Gly	Leu	Lys	His	Leu	Asp	Asn
E5		distal			E10					E15					E20	EF1		EF3	F1
				85		F			90					95					100
Leu	Lys	Gly	Thr	Phe	Ala	Lys	Leu	Ser	Glu	Leu	His	Cys	Asp	Gln	Leu	His	Val	Asp	Pro
			F5					F10			proximal		F15	FG1				FG5	G1
				105				G	110					115					120
Glu	Asn	Phe	Arg	Leu	Leu	Gly	Asn	Val	Ile	Val	Val	Val	Leu	Ala	Arg	Arg	Leu	Gly	His
			G5					G10					G15					G20	GH1
				125					130		H			135					140
Asp	Phe	Asn	Pro	Asp	Val	Gln	Ala	Ala	Phe	Gln	Lys	Val	Val	Ala	Gly	Val	Ala	Asn	Ala
	GH3	H1				H5					H10					H15			
				145															
Leu	Ala	His	Lys	Tyr	His														
	H20	HC1			HC4														

(*b*)

Figure 2
Sequence alignment of porcine haemoglobin. (*a*) α-subunits, (*b*) β-subunits. The helical segments are indicated by boxes. The helix assignments in the refined structure differ slightly from those of Katz *et al.* (1994) as follows. In the α-subunit: helix A, residues 3–18; helix B, residues 20–36 (instead of 20–35); helix C, 37–43 (36–42); helix E, 52–72 (52–71); helix F, 75–89 (80–88); helix G, 94–113 (94–112); helix H, 118–138. In the β-subunit: helix A, residues 4–16 (instead of 4–18); helix B, residues 19–35 (19–34); helix C, 36–46 (35–41); helix D, 50–56; helix E, 57–76; helix F, 80–94 (85–93); helix G, 100–119 (99–117); helix H, 123–142 (123–143).

Table 3
Comparison of structures at 2.8 and 1.8 Å resolution.

	2.8 Å structure	1.8 Å structure
Ramachandran plot (residues in disallowed region)	3	None
R.m.s. error in atomic coordinates (Luzzati, 1952) (Å)	∼0.3	∼0.15
No. of water molecules in final refinement	130	574
$R_{\rm merge}$	0.087	0.058
Electron density around Asp21β and Glu22β of helix B	None	Clear
Electron-density map in H-helix of α_2 subunit	Many breaks	No breaks
Electron-density map in all four haem groups	Unclear	Clear
R.m.s. deviation of backbone between pHb and hHb (Å)	∼0.8	∼0.8
Superimposed α subunits (r.m.s. deviation)	1.8 Å for all atoms, 0.6 Å for backbone	2.04 Å for all atoms, 0.83 Å for backbone
Superimposed β subunits (r.m.s. deviation)	1.3 Å for all atoms, 0.6 Å for backbone	1.68 Å for all atoms, 0.53 Å for backbone
Sequence alignment	Many helix differences (see Fig. 2)	

C-helix and the beginning of the CE loop (Thr41–Asn47).

The β subunit superimposes upon its sister subunit with r.m.s. deviations of 1.68 and 0.53 Å for side-chain and backbone atoms, respectively. Here, three regions of the β subunit have minor structural differences (Ser44, Phe45 and Gly46 at the end of the C-helix; Leu48 and Ser49 in the CD loop; Gln95 and Leu96 in the FG loop) and six regions have major differences [six residues at the N-terminal; residue Leu14 in the A helix; residues Val20 and Asp21 in the B helix; three residues (Met55, Gly56 and Asn57) in the D helix; two residues at the end of the E helix and the beginning of the EF loop (Lys76 and His77) and two residues at the C-terminus].

Superposition of dimer $\alpha_1\beta_1$ on dimer $\alpha_2\beta_2$ results in r.m.s. deviations of 0.75 Å for the backbone atoms and 1.87 Å for the side-chain atoms.

3.3. Haem structures

In the crystal structure of oxy-hHb, all the atoms of each haem group are planar (Shaanan, 1983), but in deoxy-hHb (Fermi *et al.*, 1984) each haem iron lies ∼0.4 Å out of the plane towards the proximal histidine ligand (His87 in the α subunit and His92 in the β subunit). In the present structure, all four Fe atoms lie in the haem planes within experimental error. Table 4 summarizes the histidine–Fe distances of three different haemoglobin structures. It is clear that the distal histidine distances are nearly equal in hHb and pHb structures, but the proximal histidine distance in the pHb structure is slightly longer (∼0.7 Å) than that of the hHb structures. Similar structures are found in aquomet horse haemoglobin (Ladner *et al.*, 1977). The models of the haem groups and the subunits with surrounding residues fit well into the electron-density map (Fig. 5).

When pHb was purified, the MetHb content was determined to be 2–3%. After lyophilization and storage, the

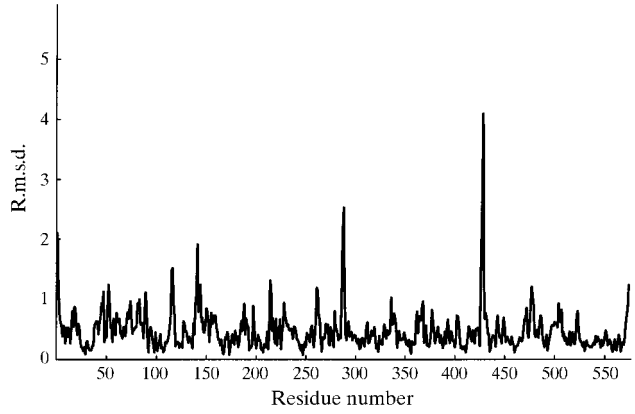

Figure 3
The r.m.s. deviation *versus* the residue number for the least-squares superposition of 2.8 Å resolution on 1.8 Å resolution structures. The five high r.m.s. deviation values indicated are the N-terminal and C-terminal of all four subunits. In the figure, 1 represents the first residue of the α_1 subunit, 142 represents the first residue of the β_1 subunit, 287 represents the first residue of the α_2 subunit and 428 represents the first residue of the β_2 subunit.

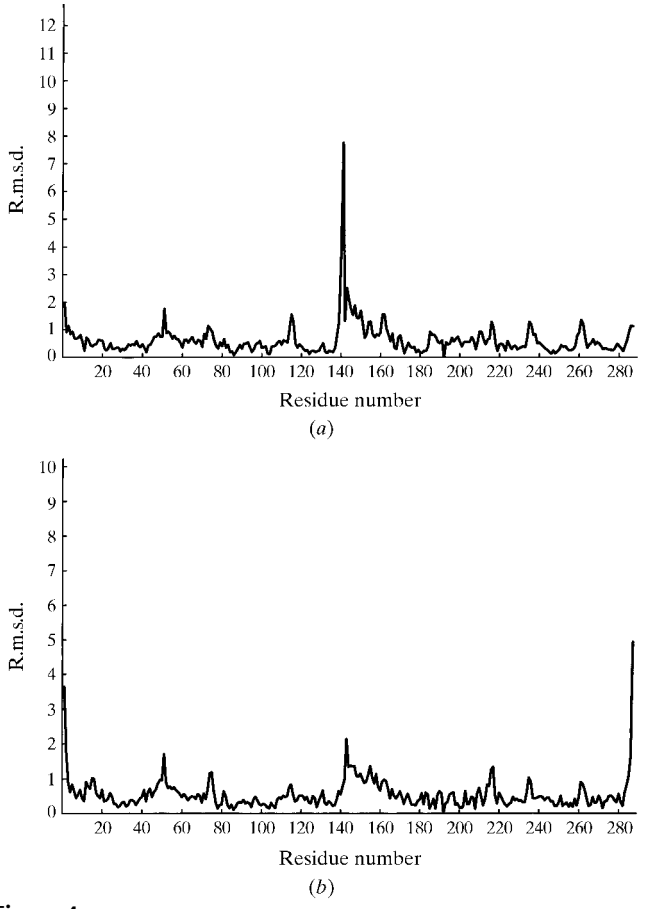

Figure 4
The plot of the least-squares superposition of the oxy-hHb on pHb structures: (*a*) $\alpha\beta$ of oxy-hHb and $\alpha_1\beta_1$ of pHb, (*b*) $\alpha\beta$ of oxy-hHb and $\alpha_2\beta_2$ of pHb. The high r.m.s. deviation values shows that both terminals of each subunit have large deviations. 1 represents the first residue of α-subunits and 142 the first residue of β subunits.

Table 4
Histidine–Fe distances in haemoglobin structure (Å).

His87 and His92 are the 'proximal histidine' in the α and β subunits, respectively. His58 and His63 are the 'distal histidine' in the α and β subunits, respectively.

Structure	α_1 subunit	β_1 subunit	α_2 subunit	β_2 subunit
pHb (1.8 Å)	His58, 4.1; His87, 2.7	His63, 4.4; His92, 2.8	His58, 4.5; His87, 2.9	His63, 4.0; His92, 2.8
pHb (2.8 Å)†	His58, 4.2; His87, 2.7	His63, 4.4; His92, 3.0	His58, 4.1; His87, 2.8	His63, 3.8; His92, 2.9
Oxy hHb‡	His58, 4.3; His87, 1.9	His63, 4.2; His92, 2.1	Same as for α_1 subunit	Same as for β_1 subunit
Deoxy hHb§	His58, 4.2; His87, 2.1	His63, 4.1; His92, 2.1	His58, 4.4; His87, 2.2	His63, 4.4; His92, 2.0

† Katz *et al.* (1994). ‡ Shaanan (1983). § Fermi *et al.* (1984).

MetHb content appeared to have increased. A 400–650 nm wavelength spectrum indicated that the MetHb content had increased to ∼10%. It should be taken into consideration that the crystallization conditions may also have some effect. When purified porcine Hb was characterized, porcine Hb exhibited a higher oxygen affinity [P_{50} = 1.3 (1) kPa] than human Hb [P_{50} = 2.0 (1) kPa] (Devenuto & Zegna, 1982). The Hill coefficient (n) of porcine Hb was calculated to be 2.16; that is, a little smaller than human Hb (2.48). The value is taken as a measure of the cooperative binding of oxygen by Hb. Accordingly, human Hb was found to have a more prominent haem–haem interaction than porcine Hb. In the $F_o - F_c$ maps of all four subunits, there is a clear electron density between the Fe atom and the distal histidine N atom in each region. This implies that there is a water molecule present. From this point of view, the present haemoglobin shows an aquomet form. This is evident because the refinement was carried out to 1.8 Å resolution in contrast to the 2.8 Å structure (Katz *et al.*, 1994). The pHb is more likely to be in the R state for the quaternery structure in the present haemoglobin. The haem groups fit very well to the $2F_o - F_c$ map (Fig. 5). The atoms of each haem group in pHb make extensive van der Waals

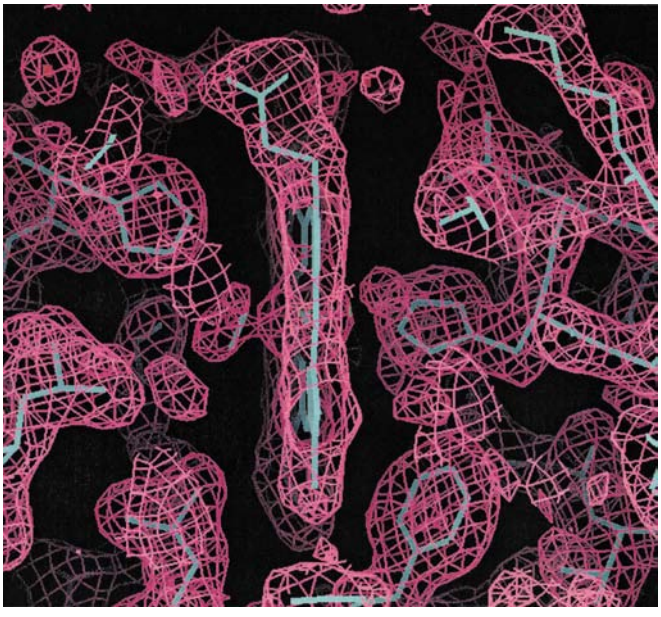

Figure 5
A $2F_o - F_c$ map of the haem group of the α_2 subunit of pHb.

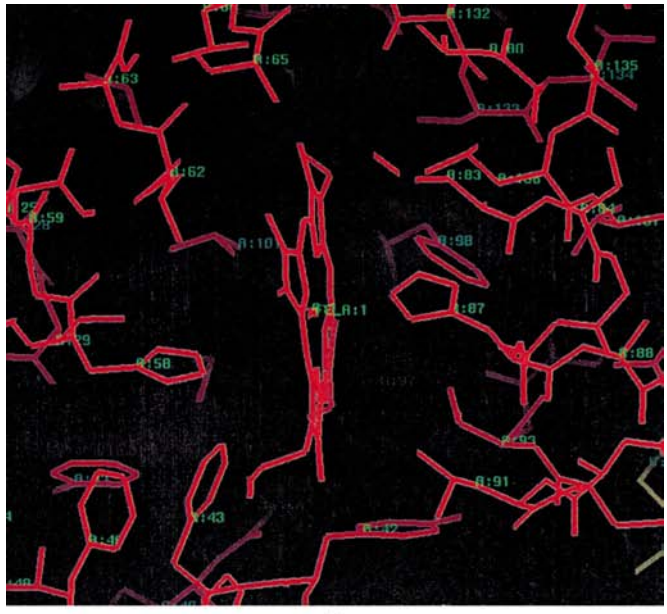

(*a*)

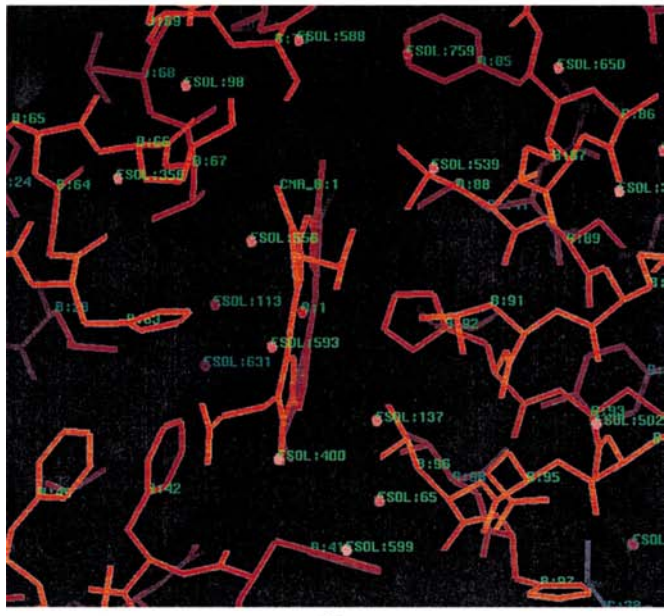

(*b*)

Figure 6
(*a*) The haem group with proximal histidine (His87), distal histidine (His58) and surrounding residues up to a radius of 4.0 Å from the α_1 subunit. (*b*) The heme group with proximal histidine (His92), distal histidine (His63) and surrounding residues up to a radius of 4.0 Å from the β_1 subunit.

contacts with neighbouring residues in the protein core (Fig. 6).

3.4. Complementarity relationship

The pHb tetramer binds together through a physical complementarity relationship. Charges on the surface of each monomer play an important role in pHb for complementary attraction, such that the entire tetramer remains stable after being isolated and purified. The electrostatic potential surfaces of the α_1 subunit of pHb calculated using the program *GRASP* (Nicholls *et al.*, 1991; Nicholls, 1993) are consistent with those obtained by Katz *et al.* (1994), but exhibit sharper contrasts in charge distribution (Fig. 7). The surface-charge distributions of mutually attracted portions between monomers were calculated using the program *INSIGHTII* (Molecular Simulation Inc., San Diego, USA) and are shown in Fig. 8. A specific binding site usually exhibits a certain small region of acidic or basic amino acids to complement its potential receptor or target. However, Figs. 8 and 9 show no such definite region, but instead show nearly uniform 'island' distributions of positive (blue), negative (red) and neutral (white) surface charges. A tentative explanation for the uniform 'island' charge distributions is as follows.

Haemoglobin (Hb) is isolated from erythrocytes and is an important component of red blood cells. The cell membrane consists of double-chain amphiphile structures that encompass the spherical bilayer. The polar ends of the double-chain amphiphiles inside the blood-cell vesicle form a complementarity relationship with the 'island' surface of the Hb (Fig. 9). Artificial blood is the final aim of our pHb structure determination. To artificially encapulate Hb with synthetic polymers or phospholipid vesicles is a great step towards the production of man-made blood. Stabilized phospholipid vesicle-encapsulated Hb (Tsuchida, 1994) indicates the successful complementarity relationship between Hb and the erythrocyte membrane.

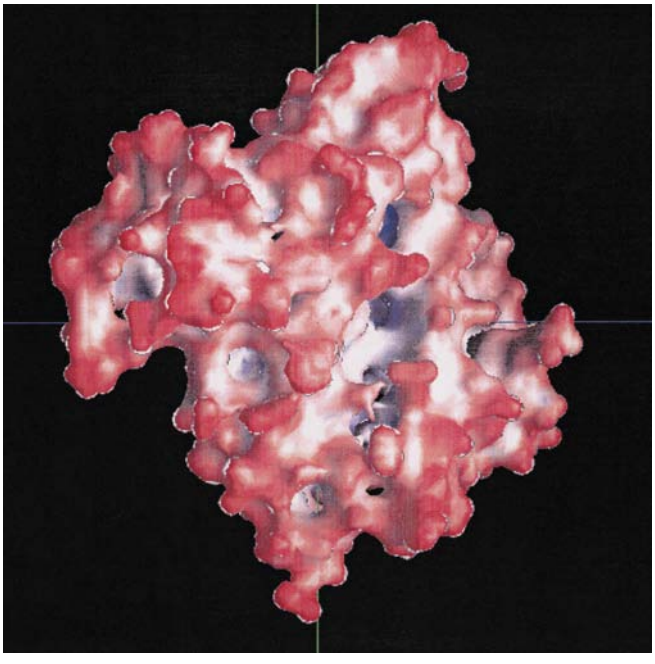

Figure 7
Electrostatic potential surface of the α_1 subunit of pHb, which shows it is similar to that of Katz *et al.* (1994). The negative, positive and neutral charges are represented by red, blue and white colours, respectively.

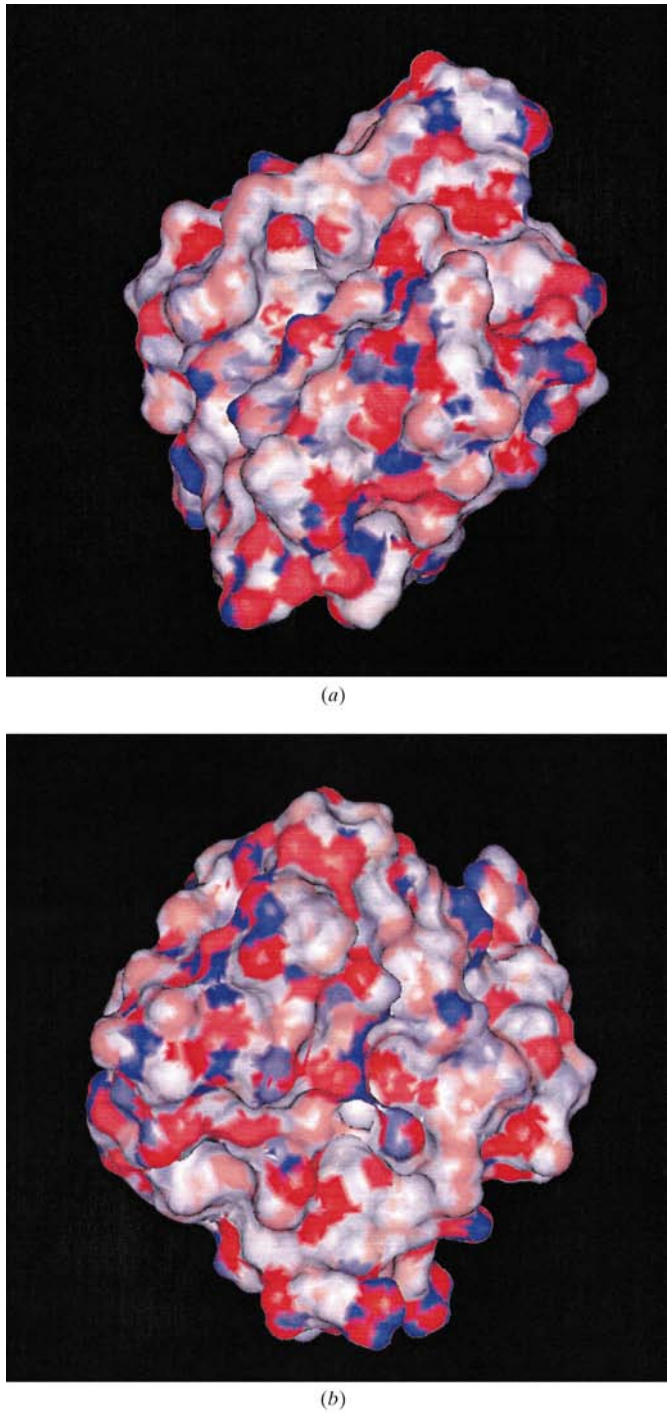

Figure 8
The surface-charge distributions (using *INSIGHTII*) of (*a*) α_1 subunit, with 180° rotation to show the complementarity to (*b*) α_2 subunit.

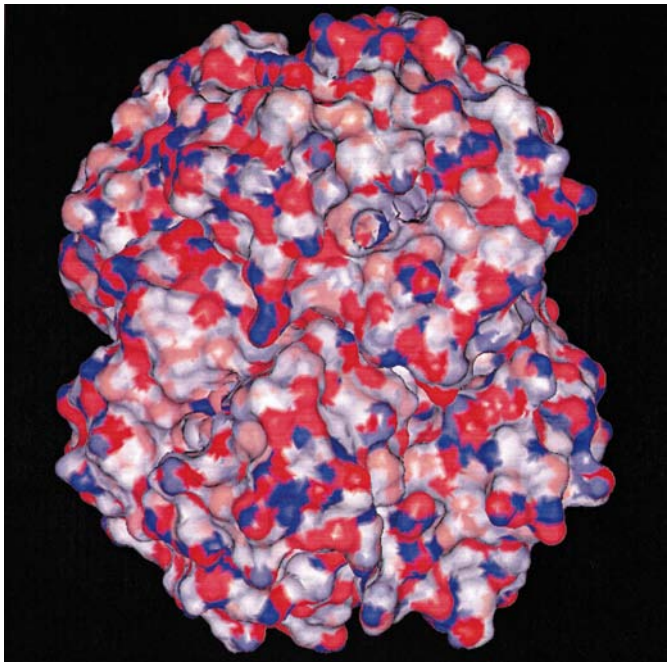

Figure 9
The surface-charge distribution of the pHb tetramer (using *INSIGHTII*). Negative charge are represented as red, positive charge as blue and neutral charge as white. Bottom, $\alpha_1\beta_1$ subunits; top, $\alpha_2\beta_2$ subunits.

The authors thank Mr Shyh-Ming Chen for setting up the computing programs. They also thank the National Science Council, Republic of China, for support under grants NSC88-2112-M007-013, NSC88-2314-B007-001 and NSC88-2811-M007-0004. They are indebted to the National Center for High-Performance Computing for use of their resources.

References

Ackers, G. K. & Smith, F. R. (1987). *Annu. Rev. Biophys. Biophys. Chem.* **16**, 583–609.

Bernstein, F. C., Koetzle, T. F., Williams, G. J. B., Meyer, E. F. Jr, Brice, M. D., Rodgers, J. R., Kennard, O., Shimanouchi, T. & Tasumi, M. (1977). *J. Mol. Biol.* **112**, 535–542.

Blow, D. M. (1958). *Acta Cryst.* **11**, 125–126.

Bolton, W. & Perutz, M. F. (1970). *Nature (London)*, **228**, 551–552.

Borgstahl, G. E. O., Rogers, P. H. & Arnone, A. (1994*a*). *J. Mol. Biol.* **236**, 817–830.

Borgstahl, G. E. O., Rogers, P. H. & Arnone, A. (1994*b*). *J. Mol. Biol.* **236**, 831–843.

Braden, B. C., Arents, G., Padlan, E. A. & Love, W. E. (1994). *J. Mol. Biol.* **238**, 42–53.

Braunitzer, F., Schrank, B., Stangl, A. & Scheithauer, U. (1978). *Hoppe-Seyler's Z. Physiol. Chem.* **359**, 137–146.

Brünger, A. T. (1992). *X-PLOR Version* 3.1. *A System for X-ray Crystallography and NMR.* New Haven, Connecticut: Yale University Press.

Camardella, L., Caruso, C., Davino, R., Diprisco, G., Rutigliano, B., Tamburrini, M., Fermi, G. & Perutz, M. F. (1992). *J. Mol. Biol.* **224**, 449–460.

Chothia, C. & Lesk, A. M. (1986). *EMBO J.* **5**, 823–826.

Clement, S., Delcros, J. G., Basu, H. S., Quash, G., Marton, L. J. & Feuerstein, B. G. (1995). *Biochem. J.* **309**, 787–791.

Coghlan, D., Jones, G., Denton, K. A., Wilson, M. T., Chan, B., Harris, R., Woodrow, J. R. & Ogden, J. E. (1992). *Eur. J. Biochem.* **207**, 931–936.

Condon, P. J. & Royer, W. E. (1994). *J. Biol. Chem.* **269**, 25259–25267.

Devenuto, F. & Zegna, A. (1982). *J. Surg. Res.* **34**, 205–212.

Ellis, P. J., Appleby, C. A., Guss, J. M., Hunter, W. N., Ollis, D. L. & Freeman, H. C. (1997). *Acta Cryst.* D**53**, 302–310.

Feola, M., Gonzalez, H., Canizaro, P. C., Bingham, D. & Periman, P. (1983). *Surg. Gynecol. Obstet.* **157**, 399–408.

Fermi, G., Perutz, M. F., Shaanan, B. & Fourme, R. (1984). *J. Mol. Biol.* **175**, 159–174.

Fermi, G., Perutz, M. F., Williamson, D., Stein, P. & Shih, D. T. B. (1992). *J. Mol. Biol.* **226**, 883–888.

Frier, J. A. & Perutz, M. F. (1977). *J. Mol. Biol.* **112**, 97–112.

Hsieh, Y. L., Lu, T. H., Lee, C. J. & Wang, B. C. (1992). *The Fourth International Conference on Biophysics and Synchrotron Radiation, Tsukuba, Japan*, p. A206.

Ippolito, J. A., Alexander, R. S. & Christianson, D. W. (1990). *J. Mol. Biol.* **215**, 457–471.

Kan, P. & Lee, C. J. (1994). *Artif. Cells Blood Substit. Immobil. Biotechnol.* **22**, 641–649.

Katz, D. S., White, S. P., Huang, W., Kumar, R. & Christianson, D. W. (1994). *J. Mol. Biol.* **244**, 541–553.

Kavanaugh, J. S., Chafin, D. R., Arnone, A., Mozzarelli, A., Rivetti, C., Rossi, G. L., Kwiatkowski, L. D. & Noble, R. W. (1995). *J. Mol. Biol.* **248**, 136–150.

Kleinschmidt, T. & Sgouros, J. G. (1987). *Biol. Chem. Hoppe-Seyler*, **368**, 579–615.

Kolatkar, P. R., Ernst, S. R., Hackert, M. L., Ogata, C. M., Hendrickson, W. A., Merritt, E. A. & Phizackerley, R. P. (1992). *Acta Cryst.* B**48**, 191–199.

Ladner, R. C., Heidner, E. J. & Perutz, M. F. (1977). *J. Mol. Biol.* **114**, 385–414.

Laskowski, R. A., MacArthur, M. W., Moss, D. S. & Thornton, J. M. (1993). *J. Appl. Cryst.* **26**, 283–291.

Lee, C. J., Kan, P. & Chen, W. K. (1992). *Artif. Cells Blood Substit. Immobil. Biotechnol.* **20**, 477–488.

Luzzati, P. V. (1952). *Acta Cryst.* **5**, 802–810.

McPherson, A. (1982). *Preparation and Analysis of Protein Crystals*, 1st ed., pp 96–97. New York: John Wiley & Sons.

Mitchell, D. T., Ernst, S. R. & Hackert, M. L. (1995). *Acta Cryst.* D**51**, 760–766.

Mitchell, D. T., Ernst, S. R., Wu, W. X. & Hackert, M. L. (1995). *Acta Cryst.* D**51**, 647–653.

Moulton, D. P., Joshi, A. A., Morris, A. & Mcdonald, M. J. (1994). *Biochem. Biophys. Res. Commun.* **204**, 956–961.

Nicholls, A. (1993). *GRASP: Graphical Representation and Analysis of Surface Properties.* Columbia University, New York, USA.

Nicholls, A., Sharp, K. A. & Honig, B. (1991). *Proteins Struct. Funct. Genet.* **11**, 281–296.

Osawa, Y., Fellows, C. S., Meyer, C. A., Woods, A., Castoro, J. A., Cotter, R. J., Wilkins, C. L. & Highet, R. J. (1994). *J. Biol. Chem.* **269**, 15481–15487.

Paoli, M., Liddington, R., Tame, J., Wilkinson, A. & Dodson, G. (1996). *J. Mol. Biol.* **256**, 775–792.

Pechik, I., Ji, X. H., Fidelis, K., Karavitis, M., Moult, J., Brinigar, W. S., Fronticelli, C. & Gilliland, G. L. (1996). *Biochemistry*, **35**, 1935–1945.

Pellegrini, M., Giardina, B., Olianas, A., Sanna, M. T., Deiana, A. M., Salvadori, S., Diprisco, G., Tamburrini, M. & Corda, M. (1995). *Eur. J. Biochem.* **234**, 431–436.

Perutz, M. F. (1978). *Sci. Am.* **239**, 91–125.

Perutz, M. F., Fermi, G., Poyart, C., Pagnier, J. & Kister, J. (1993). *J. Mol. Biol.* **233**, 536–545.

Richard, V., Dodson, G. G. & Mauguen, Y. (1993). *J. Mol. Biol.* **233**, 270–274.

Rizzi, M., Wittenberg, J. B., Coda, A., Fasano, M., Ascenzi, P. & Bolognesi, M. (1994). *J. Mol. Biol.* **244**, 86–99.

Rossmann, M. G. & Blow, D. M. (1962). *Acta Cryst.* **15**, 24–31.
Royer, W. E. (1994). *J. Mol. Biol.* **235**, 657–681.
Royer, W. E., Heard, K. S., Harrington, D. J. & Chiancone, E. (1995). *J. Mol. Biol.* **253**, 168–186.
Ryan, T. M., Townes, T. M., Reilly, M. P., Asakura, T., Palmiter, R. D., Brinster, R. L. & Behringer, R. R. (1990). *Science*, **247**, 566–568.
Shaanan, B. (1983). *J. Mol. Biol.* **171**, 31–59.
Silva, M. M., Rogers, P. H. & Arnone, A. (1992). *J. Biol. Chem.* **267**, 17248–17256.
Tsuchida, E. (1994). *Artif. Cells Blood Substit. Immobil. Biotechnol.* **22**, 467–477.
Vandegriff, K. D. & Winslow, R. M. (1991). *Chem. Ind.* **14**, 497–504.
Waller, D. A. & Liddington, R. C. (1990). *Acta Cryst.* B**46**, 409–418.
Wang, Y. C., Lee, C. J., Chen, W. K., Huang, C. I., Chen, W. F., Chen, G. J. & Lin, S. Z. (1996). *Artif. Cells Blood Substit. Immobil. Biotechnol.* **24**, 35–42.
Wireko, F. C. & Abraham, D. J. (1991). *Proc. Natl Acad. Sci. USA*, **88**, 2209–2211.
Yamauchi, K., Ochiai, T. & Usuki, I. (1992). *Biochim. Biophys. Acta*, **1171**, 81–87.
Yang, J., Kloek, A. P., Goldberg, D. E. & Mathews, P. S. (1995). *Proc. Natl Acad. Sci. USA*, **92**, 4224–4228.
Zhang, J., Hua, Z. Q., Tame, J. R. H., Lu, G. Y., Zhang, R. J. & Gu, X. C. (1996). *J. Mol. Biol.* **255**, 484–493.